NASA TECHNICAL NOTE

NASA TN D-5585

C. 1

NASA TN D-5585

ALPHA-GAMMA ANGULAR CORRELATIONS IN THE REACTION NICKEL-58 $\left(\alpha,\alpha'\gamma_{1.452\mathrm{MeV}}\right)$

by Norton Baron, Regis Leonard, and William M. Stewart

Lewis Research Center
Cleveland, Ohio

NATIONAL AERONAUTICS AND SPACE ADMINISTRATION • WASHINGTON, D. C. • FEBRUARY 1970

1. Report No. NASA TN D-5585	2. Government Accession No.	3. Recipient's Catalog No.
4. Title and Subtitle ALPHA-GAMMA ANGULAR CORRELATIONS IN THE REACTION NICKEL-58 $(\alpha, \alpha' \gamma_{1.452 MeV})$		5. Report Date February 1970
		6. Performing Organization Code
7. Author(s) Norton Baron, Regis Leonard, and William M. Stewart		8. Performing Organization Report No. E-5142
9. Performing Organization Name and Address Lewis Research Center National Aeronautics and Space Administration Cleveland, Ohio 44135		10. Work Unit No. 129-02
		11. Contract or Grant No.
12. Sponsoring Agency Name and Address National Aeronautics and Space Administration Washington, D.C. 20546		13. Type of Report and Period Covered Technical Note
		14. Sponsoring Agency Code
15. Supplementary Notes		

16. Abstract

Differential cross sections for elastic scattering and excitation of the 1.452-MeV 2^+ state of nickel-58 were measured for 41-MeV incident alpha particles. The angular correlation between the inelastically scattered alpha particles and the gamma rays emitted in the plane of original scattering in the subsequent nuclear decay were measured also for the excitation of the 1.452-MeV state. The data are compared with optical model calculations of the elastic cross sections and distorted waves Born approximation calculations of the 2^+ cross sections and correlation symmetry angles.

17. Key Words (Suggested by Author(s)) $^{58}Ni(\alpha, \alpha' \gamma_{1.452 MeV})$ Alpha-gamma correlations	18. Distribution Statement Unclassified - unlimited

19. Security Classif. (of this report)	20. Security Classif. (of this page)	21. No. of Pages	22. Price*
Unclassified	Unclassified	34	$3.00

*For sale by the Clearinghouse for Federal Scientific and Technical Information
Springfield, Virginia 22151

ALPHA-GAMMA ANGULAR CORRELATIONS IN THE REACTION NICKEL-58 $(\alpha, \alpha'\gamma_{1.452MeV})$

by Norton Baron, Regis Leonard, and William M. Stewart

Lewis Research Center

SUMMARY

Differential cross sections for elastic scattering and excitation of the 1.452-MeV 2^+ state of nickel-58 were measured for 41-MeV incident alpha particles over the angular range from 10° to 141°. The angular correlation between the inelastically scattered alpha particles and the gamma rays emitted in the plane of original scattering in the subsequent nuclear decay were measured also for the excitation of the 1.452-MeV state of nickel-58. The symmetry angles of the gamma distribution were extracted from the correlation data at center of mass scattering angles between 12° and 68°. The measured symmetry angles were close to the adiabatic prediction over the range of alpha-particle scattering angles studied, except for rapid reverse rotations in the region of 17° and 27.5°. These results are compared with optical model calculations of the elastic cross sections and distorted waves Born approximation calculations of the 2^+ cross sections and symmetry angles. Several optical model potentials agreed satisfactorily with the data. However, calculations using six-parameter decoupled potentials gave better agreement with the data than the four-parameter coupled potentials which are conventionally used for the analysis of alpha-particle scattering.

INTRODUCTION

In earlier work, extensive optical model calculations were performed for the cross sections of 42-MeV alpha particles elastically scattered from isotopes of tin (ref. 1) and tellurium (ref. 2). These data could be satisfactorily described by the use of any one of many equally good potentials having real well depths ranging from about 40 to several hundred MeV, provided that the potentials at the nuclear surface are similar (ref. 2). This nonuniqueness of a suitable optical model potential for alpha-particle scattering also exists for lighter nuclei except that only discrete sets of parameters are found (refs. 3 and 4).

The differential cross section (refs. 5 and 6) for inelastic scattering

$$\frac{d\sigma}{d\Omega} = \sum_{m} \frac{|F_{Lm}|^2}{2L + 1} \tag{1}$$

is calculated by using the distorted-waves Born approximation (DWBA), with the distorted waves being generated by the optical potential used to describe the elastic scattering. Equation (1) shows that the phases of the transition amplitudes F_{Lm} are unimportant in the cross-section calculation which involves only the sum of the squares of F_{Lm}. It is hoped that the measurement of another observable, which depends on the phases of the transition amplitudes, will eliminate the ambiguities in the optical potentials which describe the elastic scattering of medium energy alpha particles.

An observable that is sensitive to the phases of the transition amplitudes is the angular correlation between the inelastically scattered alpha particle and the gamma ray emitted in the subsequent decay of the residual nucleus (ref. 7). In the present study this correlation is measured as a function of the scattered alpha angle for gamma angles in the plane of original scattering. A DWBA calculation of this correlation is performed using the several optical model potentials that successfully describe the elastic scattering from the target nucleus.

The angular correlation study presented here is for the target nucleus nickel-58 (^{58}Ni). This is an extension of similar studies on magnesium-24 (^{24}Mg) (ref. 7). In view of the preceding discussion, it is desirable to determine the sensitivity, if any, in different mass regions of the periodic table of such a measurement for the determination of a unique optical model potential. Furthermore, since very few alpha-gamma angular correlation measurements have been reported, such experiments are interesting in themselves in order to gain more insight into this phenomenon.

SYMBOLS

A	magnitude of isotropic component of alpha-gamma correlation function
$A^{1/3}$	atomic mass number to the one-third power
a_x	diffuseness parameter in Woods-Saxon form factor
B	magnitude of anisotropic component of alpha-gamma correlation function
F_{Lm}	reduced transition amplitude

$f(r, r_x, a_x)$	Woods-Saxon form factor of nuclear optical potential
$\langle j_1 m_1 j_2 m_2 \vert JM \rangle$	Clebsch-Gordan coefficient for addition of angular moments $j_1 m_1$ and $j_2 m_2$ to obtain a resultant JM
k	linear momentum in units of $\hbar$
L	angular momentum transfer
l	multipolarity of γ-ray de-excitation
m	projection of angular momentum onto z-axis
R	mean radius of nuclear potential, thus mean interaction radius
r_x	distance measured from center of nucleus
U(r)	optical potential
V	strength of real part of nuclear optical potential
$V_C(r)$	Coulomb potential
W	strength of imaginary part of nuclear optical potential
$W(\theta_\alpha, \theta_\gamma)$	correlation function in reaction plane
$Y_l^m(\theta, \varphi)$	spherical harmonic of order l, m
β_2	quadrupole nuclear deformation parameter of vibrational collective model
θ_α	alpha particle scattering angle in center of mass system relative to incident-beam direction
θ_γ	angle of emission of gamma ray, relative to incident-beam direction
θ_0	symmetry angle of alpha-gamma correlation function
$d\sigma/d\Omega$	differential cross section

EXPERIMENTAL ARRANGEMENT

Beam Handling

The energy of the extracted alpha-particle beam of the NASA 1.5-meter cyclotron is 41.1±0.2 MeV. The method for the determination of the extracted alpha-particle energy was reported previously (ref. 1). The principal considerations in the design of the beam transport system for the angular correlation measurements were the reduction of the background of neutrons and gamma rays in the scattering room. The energy resolution that could be attained in the analysis of scattered alpha particles in the correlation measurement was of secondary interest.

A schematic diagram of the beam transport system and the experimental area is shown in figure 1. The extracted alpha beam was focused onto slit S_1, the source slit for the 60^0 magnet, which served principally to bend the beam away from the original beam line, thereby preventing neutrons travelling along the original beam line from entering the target area. Slit S_2, located 56 centimeters from the exit of the magnet and at a width of 1 millimeter, together with slit S_3, which was 1 millimeter wide, defined the direction of the beam incident on the target. To reduce the gamma-ray background in the target area,

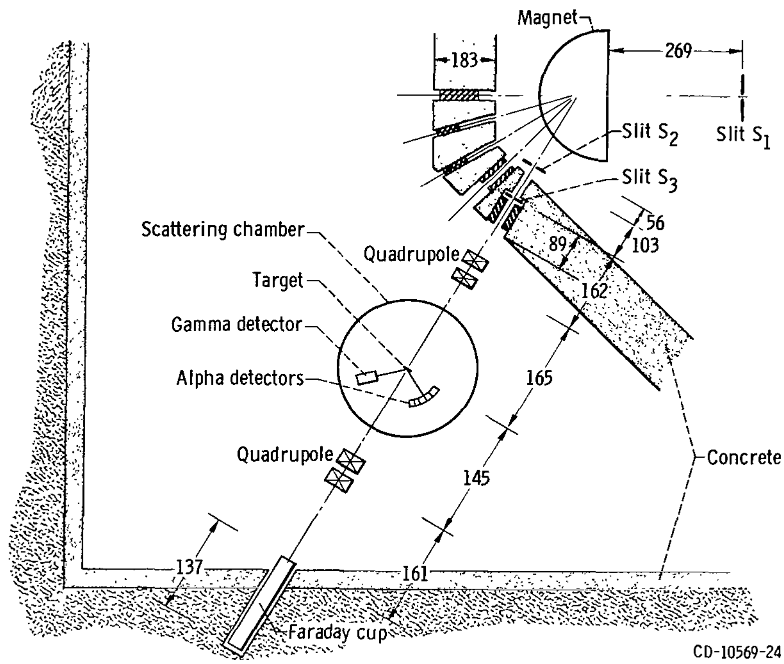

Figure 1. - Schematic diagram of scattering system. (All dimensions are in cm.)

slit S_3 was located within a concrete wall and was followed by a cylinder of lead 90 centimeters long with a 1.9-centimeter diameter hole to permit passage of the incident beam. Slit S_3, the last defining aperture through which the incident alpha particles pass prior to reaching the target was 327 centimeters from the target. Other than the ^{58}Ni target, the remaining principal source of background was the beam stopper located 137 centimeters deep inside a concrete wall and 443 centimeters from the target as shown in figure 1.

The beam handling system for the cross section measurements was similar to that described in a previous report (ref. 1).

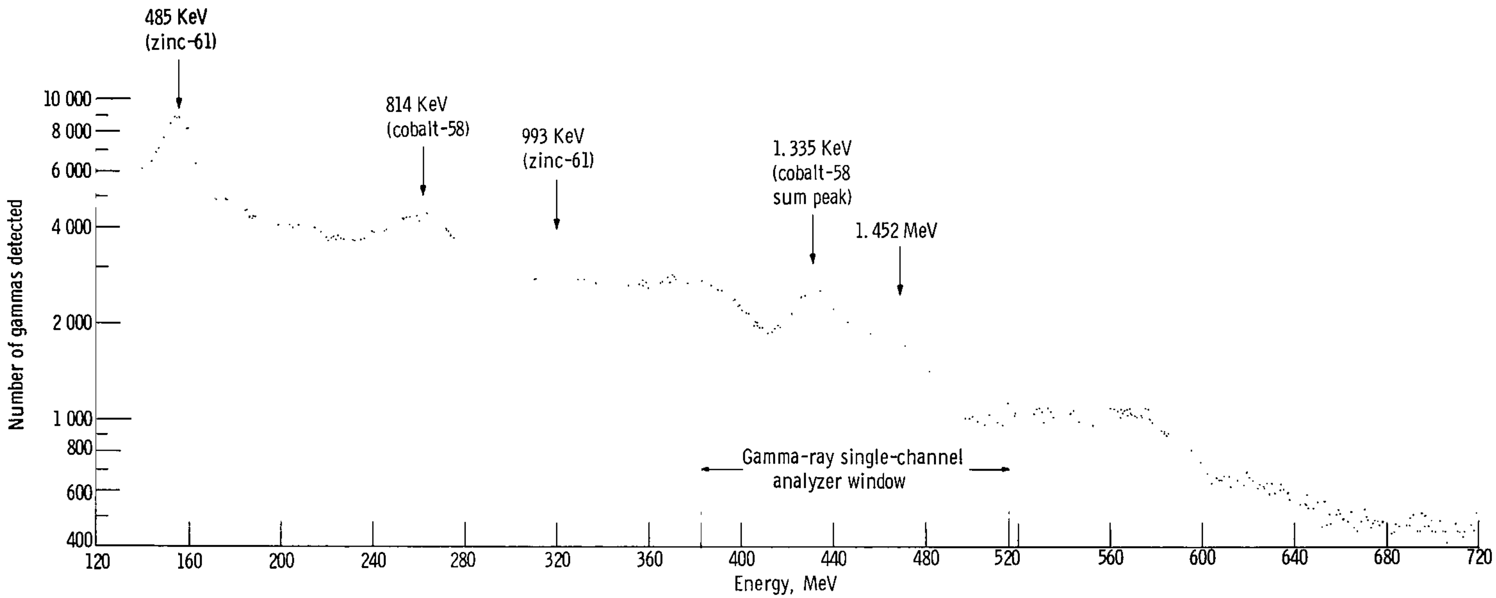

Figure 2. - Gamma-ray singles spectrum for the reaction nickel-58 (α, γ) using 41-MeV incident alpha particles.

Detectors

Charged particles were detected by lithium drifted silicon semiconductor counters which were manufactured at Lewis (ref. 8). Scattered alpha particles were counted at 10 different angles simultaneously by using 10 counters, mounted at 4° intervals in a multidetector mount similar to that previously described in reference 8. The angular resolution for the cross section and correlation measurements was 1° except at certain angles where the correlation measurements necessitated 0.25°. The mean scattering angle was known to $\pm 0.06^{\circ}$.

Gamma rays were detected by a 7.62- by 7.62-centimeter sodium iodide (T1) crystal. The front face of the crystal was 12.7 centimeters from the target, resulting in a 35° angle subtended by the detector. The gamma spectrum obtained by bombardment of the ^{58}Ni target by 41-MeV incident alpha particles is shown in figure 2.

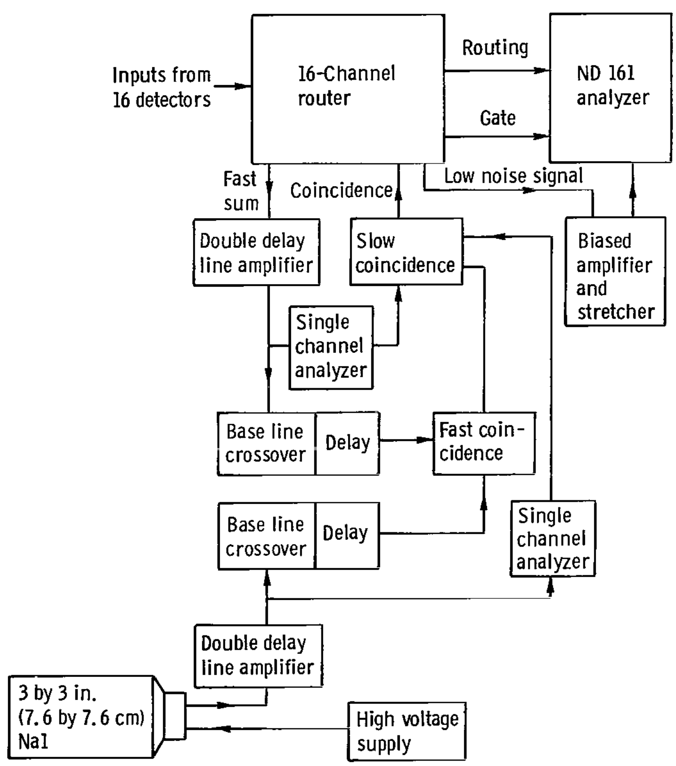

Figure 3. - Multidetector coincidence arrangement using 16-channel router.

Electronics

A block diagram of the electronic system used for the correlation measurement is shown in figure 3. The individual alpha-particle signals are amplified, mixed, and then fanned out to timing and energy analysis circuits. The signals fed to the energy analysis circuit are shaped to provide good energy resolution, while those for the timing circuit are unshaped in order to provide good time resolution. The generation of a suitable routing signal enables the alpha-particle signals from each counter to be analyzed and stored in one of the sixteen 256-channel subgroups of the pulse height analyzer, provided they occur in time coincidence with a gamma ray of the proper energy as determined by a single-channel analyzer. The coincidence circuit for the experiment was a standard parallel fast-slow arrangement with a resolving time of 50 nanoseconds, which is smaller than the 100-nanosecond time between the beam pulses of the cyclotron. The 16-channel router was described in a previous report (ref. 9).

The cross section measurement involves the same electronics as that of the preceding description for the correlation measurement except that the gamma-ray coincidence was not required.

Cross-Section Measurements

Cross sections were measured for elastic scattering ($10^{\circ} < \theta_{\alpha} < 141^{\circ}$) and for the excitation of the first excited level (1.452 MeV) of ^{58}Ni ($17^{\circ} < \theta_{\alpha} < 141^{\circ}$). The incident charge was measured using a Faraday cup. The experimental differential cross sections and their associated statistical uncertainties are listed in table I. Energy resolutions for the cross-section measurements were typically 100 keV full width at half maximum.

The principal sources of error in the determination of absolute cross sections were the statistical uncertainties and the determination of the target thickness. For both the elastic and inelastic cross sections, the statistical uncertainties are generally less than 5 percent for scattering angles less than 90° and between 5 and 10 percent for scattering angles between 90° and 141° (see table I). The target was an isotopically enriched self-supporting ^{58}Ni foil having an isotopic abundance of 99.95 percent. The foil was furnished by the Oak Ridge Laboratory Isotopes Development Center. The value of the target thickness used for the cross-section calculations was 0.974 milligram per square centimeter as determined from the measured energy degradation of 8.78-MeV alpha particles from a natural radioactive source. The principal uncertainty in this determination is the calculated stopping power (ref. 10). An alternate determination of the target thickness was provided by a direct weighing of a known area of the target foil which gave a value of 0.905 milligram per square centimeter. The weight of the foil was supplied by the target fabricator.

TABLE I. - DIFFERENTIAL CROSS SECTIONS FOR SCATTERING OF 41-MeV ALPHA PARTICLES FROM NICKEL-58

(a) Elastic scattering

Center of mass scattering angle, θ_{cm}, deg	Differential cross section, $d\sigma/d\Omega$, mb/sr	Center of mass scattering angle, θ_{cm}, deg	Differential cross section, $d\sigma/d\Omega$, mb/sr	Center of mass scattering angle, θ_{cm}, deg	Differential cross section, $d\sigma/d\Omega$, mb/sr
10.69	34 400±200	57.20	1.23±0.04	101.92	0.0728±0.0043
12.82	6 410±40	59.28	2.57±0.04	103.90	.0431±0.0033
14.96	2 930±10	61.36	2.43±0.06	105.88	.0287±0.0027
17.09	2 430±10	63.43	1.22±0.03	107.84	.0195±0.0022
19.22	1 230±10	65.50	0.411±0.018	109.81	.0274±0.0026
21.35	385±3	67.56	.399±0.014	111.77	.0261±0.0026
23.48	174±2	69.62	.812±0.025	113.72	.0333±0.0027
25.61	234±3	71.67	.965±0.021	115.67	0.0258±0.0025
27.74	206±2	73.72	.923±0.027	117.62	.0305±0.0025
29.86	95.4±0.9	75.77	.621±0.017	119.56	.0210±0.0023
31.98	14.3±0.1	77.81	0.294±0.015	121.50	.0165±0.0019
34.10	13.5±0.1	79.84	.163±0.009	123.43	.0139±0.0019
36.21	32.4±0.2	81.88	.189±0.012	125.36	.0127±0.0015
38.33	33.4±0.1	83.90	.285±0.012	127.28	.0183±0.0020
40.44	15.0±0.1	85.92	.299±0.016	129.20	0.0224±0.0019
42.55	1.99±0.03	87.94	.232±0.011	131.12	.0259±0.0024
44.65	1.22±0.04	89.95	.128±0.010	133.03	.0222±0.0019
46.75	6.20±0.06	91.96	0.0778±0.0062	134.94	.0175±0.0020
48.85	7.56±0.09	93.96	.0497±0.0050	136.85	.0114±0.0014
50.94	4.68±0.05	95.96	.0540±0.0037	138.75	0.00983±0.00150
53.03	1.24±0.04	97.95	.0766±0.0044	140.65	.00998±0.00131
55.12	0.138±0.009	99.94	.0874±0.0047		

TABLE I. - Concluded. DIFFERENTIAL CROSS SECTIONS FOR SCATTERING OF 41 MeV ALPHA PARTICLES FROM NICKEL-58

(b) Inelastic scattering to 1.452-MeV level of nickel-58

Center of mass scattering angle, θ_{cm}, deg	Differential cross section, $d\sigma/d\Omega$, mb/sr	Center of mass scattering angle, θ_{cm}, deg	Differential cross section, $d\sigma/d\Omega$, mb/sr	Center of mass scattering angle, θ_{cm}, deg	Differential cross section, $d\sigma/d\Omega$, mb/sr
17.11	3.17±0.67	61.42	0.281±0.019	103.98	0.0630±0.0040
19.25	12.5±0.8	63.50	.518±0.016	105.95	.0749±0.0044
21.38	24.2±0.9	65.57	.644±0.022	107.92	.0679±0.0042
23.51	17.1±0.7	67.63	.589±0.017	109.88	.0574±0.0038
25.64	3.82±0.34	69.69	.403±0.018	111.84	.0441±0.0032
27.77	1.52±0.15	71.74	.268±0.011	113.80	.0368±0.0028
29.90	5.84±0.21	73.80	.213±0.013	115.74	.0282±0.0026
		75.84	.281±0.012		
32.02	7.17±0.09	77.88	.322±0.016	117.69	0.0262±0.0024
34.14	4.10±0.06			119.63	.0273±0.0026
36.26	1.11±0.04	79.92	0.297±0.012	121.57	.0314±0.0026
38.37	.485±0.020	81.95	.225±0.013	123.50	.0343±0.0029
40.49	1.95±0.05	83.98	.181±0.009	125.42	.0330±0.0023
42.60	3.13±0.04	86.00	.126±0.010	127.35	.0220±0.0022
44.70	2.51±0.05	88.02	.136±0.008	129.27	.0167±0.0017
		90.03	.133±0.010		
46.80	0.923±0.023	92.04	.164±0.009	131.18	0.00971±0.00148
48.90	.322±0.017	94.04	.131±0.009	133.09	.0111±0.0014
51.00	.669±0.019	96.04	.106±0.005	135.00	.0127±0.0017
53.09	1.34±0.04			136.90	.0176±0.0017
55.18	1.31±0.03	98.03	0.0809±0.0045	138.80	.0167±0.0020
57.27	.853±0.030	100.02	.0651±0.0040	140.70	.0143±0.0016
59.35	.346±0.014	102.00	.0593±0.0039		

Because of the difference of these two alternate measurements, an 8 percent uncertainty is attributed to the accuracy of the target thickness. Other small errors result from an imperfect measurement of the total incident charge and of the solid angle subtended by the detectors. These errors are estimated to add less than 1 percent to those described previously.

Angular Correlation Measurements

The correlation function for gammas emitted in the reaction plane is given by (ref. 11) as

$$W(\theta_\alpha, \theta_\gamma) = \sum_{\substack{m_1 m_1' \\ l m}} F^*_{Lm_1} F_{Lm_1'} \langle 2l m, Lm_1' | Lm_1 \rangle \langle L1, L - 1 | 2l o \rangle Y^m_{2l}(\theta_\gamma \pi) \tag{2}$$

The correlation function is sensitive to the phases of the transition amplitudes. The coordinate system used is spherical with the polar axis along the incident-beam direction and the azimuthal angle measured from the plane determined by the scattered alpha particles. The azimuthal angle was equal to π for all gamma rays measured in this work.

For the sequence of spins investigated here ($0^+ \rightarrow 2^+ \rightarrow 0^+$), equation (2) reduces to (ref. 12)

$$W(\theta_\alpha, \theta_\gamma) = A + B \sin^2 2(\theta_\gamma - \theta_0) \tag{3}$$

The forms of equations (2) and (3) are independent of the reaction mechanism since they involve only conservation of angular momentum considerations. The details of the reaction mechanism change only the magnitudes of A, B, and θ_0 in equation (3). The quantities that are determined from the correlation measurement are the symmetry angle θ_0, defined in equation (3) as the position of the valley in the correlation pattern, and the ratio of the isotropic to anisotropic magnitudes, A/B.

The chance coincidences counted for the 1.452-MeV state in the coincidence spectrum were calculated by assuming that the ratio of chance coincidences for the 1.452-MeV and the elastic states was equal to the ratio of their cross sections. Of course, all elastically scattered alpha particles observed in the coincidence spectrum are chance events. The cross-section ratios were determined from a singles run preceding each coincidence run. Shown in figure 4 are such spectra of a typical singles and coincidence run. The enhancement of the 2^+ level relative to the elastic peak in the coincidence spectrum is

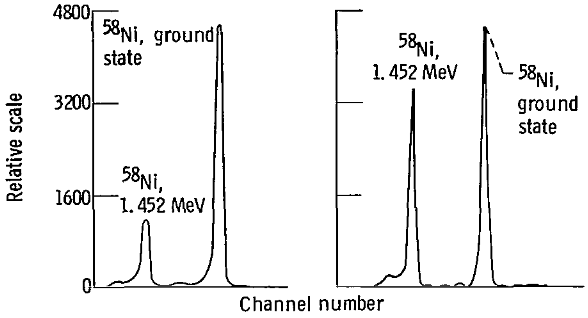

(a) Singles spectrum. (b) Coincidence spectrum.

Figure 4. - Alpha scattering spectra for the reaction nickel-58 (α, α').

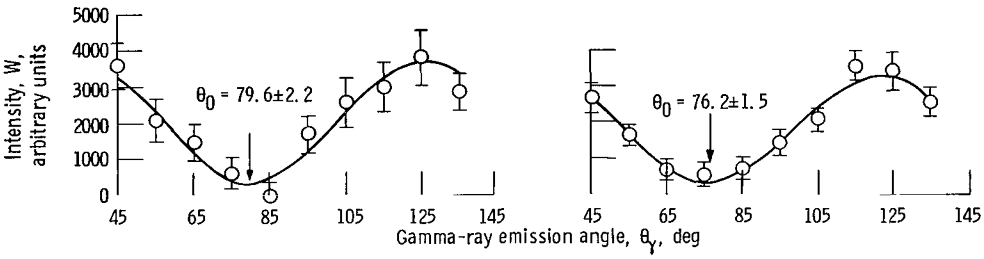

(a) Alpha-particle center of mass scattering angle, 23.48°; ratio of isotropic to anisotropic components, 0.117±0.067.

(b) Alpha-particle center of mass scattering angle, 34.10°; ratio of isotropic to anisotropic components, 0.128±0.048.

Figure 5. - Least squares fits to two sets of correlation data using function $W = A + B \sin^2 2(\theta_\gamma - \theta_0)$.

noted. The true- to chance-coincidence ratio for most of the coincidence runs was 1 to 1 or slightly less using incident currents of about 15 nanoamperes. For each correlation pattern at a given alpha scattering angle, 10 such coincidence spectra were obtained at gamma angles between 45° and 135° in steps of 10°. The method of reduction of these raw data was described previously (ref. 7). In the correlation experiment reported here, the incident charge was measured using a monitor counter.

In figure 5 are pictured several typical correlation patterns showing the angular distribution of the de-excitation gammas detected in the scattering plane coincident with alpha particles emitted at some angle. In order to determine the values of A/B and θ_0 for each alpha particle scattering angle, the function $W(\theta_\alpha, \theta_\gamma)$ of equation (3) is fitted by a least squares analysis (ref. 7) to the correlation data, and then corrected for the effects of the finite geometry of the gamma detector using the method of Rose (ref. 13). Typical least squares fits to the experimental correlation patterns are also shown in figure 5. The values of the symmetry angles θ_0 and A/B ratios determined are listed in table II, and the symmetry angle data are shown graphically in figure 6.

TABLE II. - ANGULAR CORRELATION PARAMETERS

Alpha-particle center of mass scattering angle, θ_{cm}, deg	Gamma-ray symmetry angle, θ_0, deg	Ratio of isotropic to anisotropic component, A/B	Alpha-particle center of mass scattering angle, θ_{cm}, deg	Gamma-ray symmetry angle, θ_0, deg	Ratio of isotropic to anisotropic component, A/B
12.82	76.41±5.20	0.522±0.249	36.21	66.06±7.50	0.233±0.204
14.96	83.94±3.65	.164±0.104	40.44	57.37±7.88	.349±0.292
16.02	81.86±4.28	.121±0.120	42.54	68.13±2.28	0±0.070
18.16	60.72±3.48	.038±0.098	44.65	76.62±6.03	.021±0.167
19.22	80.87±4.10	.285±0.127	46.75	64.50±6.65	0±0.233
20.29	72.84±2.19	0.186±0.069	48.85	68.05±56.4	1.39±6.17
21.35	76.41±2.75	.111±0.084	50.94	61.28±10.2	.241±0.338
22.42	77.59±3.27	0±0.092	53.03	57.25±9.07	.266±0.302
23.48	79.57±2.22	.0415±0.059	55.12	60.68±7.66	0±0.221
24.55	82.11±3.12	.079±0.085	57.20	75.48±10.03	.751±0.605
25.61	75.16±4.17	0.105±0.091	59.28	60.97±23.50	0±0.670
26.67	95.26±7.70	.088±0.213	61.36	8.79±12.34	0±0.491
27.73	101.13±6.00	.762±0.750	63.43	80.26±12.51	0±0.681
29.86	69.82±2.69	.022±0.074	65.49	74.66±25.33	0±1.179
31.98	75.24±2.93	.162±0.060	67.56	51.78±27.33	.124±0.778
34.10	76.16±1.53	.052±0.043			

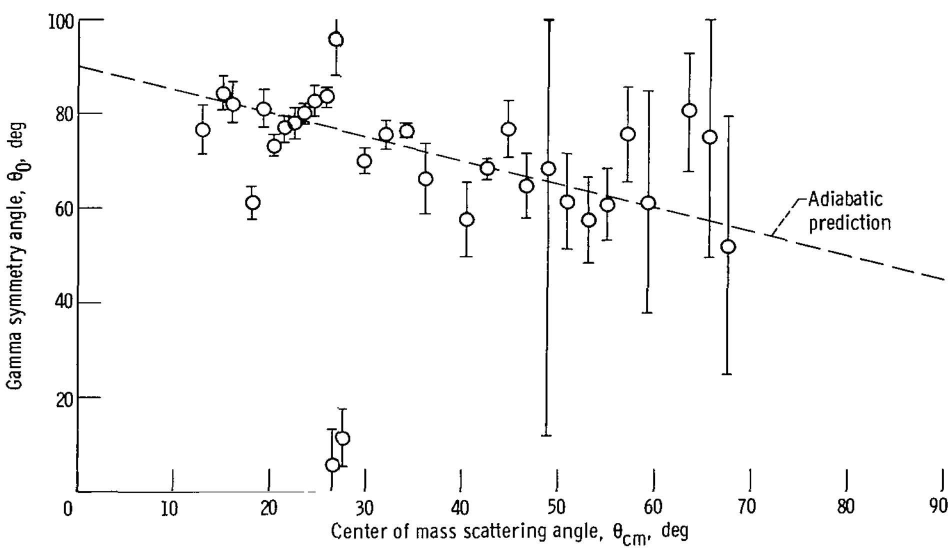

Figure 6. - Alpha-gamma angular correlation symmetry angles measured in the reaction plane for the reaction nickel-58 (α, $\alpha'\gamma_{1.452\ MeV}$) nickel-58.

The A/B ratios are not shown graphically since in most cases the errors exceed the value of the ratio. This is because of the statistics that could be obtained. This effect is more drastic for the determination of the A/B ratios than for the symmetry angles since they are the computed ratio of two measured quantities, each of which suffers independently from poor statistical accuracy.

Optical Model Potential

The optical model potential (ref. 14) used for most of the analysis of these data can be written as

$$U(r) = V_C(r) - Vf(r, r_o, a_o) - iWf(r, r_i, a_i) \tag{4}$$

where $V_C(r)$ is the Coulomb potential between the incident alpha particle and the scattering nucleus, which is assumed to be a uniformly charged sphere of radius 1.25 $A^{1/3}$ femtometers, and $f(r, r_x, a_x)$ denotes the Woods-Saxon radial form factor and has the form

$$f(r, r_x, a_x) = \left[1 + \exp\left(\frac{r - r_x A^{1/3}}{a_x}\right)\right]^{-1} \tag{5}$$

The potential (eq. (4)) has six independent parameters. However, some of the analysis was made with a four-parameter optical potential obtained by setting $r_o \equiv r_i$ and $a_o \equiv a_i$ in equation (4).

Optical Model Analysis

The elastic cross-section calculations were performed with an optical model computer program (ref. 15). The automatic search provision for the six-parameter potential was written by Davidon (ref. 16) and adapted for use at NASA Lewis by Volkin and Giamati (unpublished). The independent parameters of the optical potential are varied in order to minimize the quantity χ^2/N. This is defined as

$$\frac{\chi^2}{N} = \frac{\displaystyle\sum_{i=1}^{N} \left| \frac{\sigma_{exp}(\theta_i) - \sigma_{calc}(\theta_i)}{\Delta\sigma_{exp}(\theta_i)} \right|^2}{N} \tag{6}$$

where $\sigma_{exp}(\theta_i)$ are the measured differential cross sections at angle θ_i, $\Delta\sigma_{exp}(\theta_i)$ are the associated experimental uncertainties, $\sigma_{calc}(\theta_i)$ are the calculated values, and N is the number of experimental data points. In all the analyses of the elastic data, the experimental uncertainties $\Delta\sigma_{exp}(\theta_i)$ were taken to be 5 percent for all alpha scattering

TABLE III. - RESULTS OF OPTICAL MODEL CALCULATIONS FOR 41-MeV ALPHA PARTICLES SCATTERED BY NICKEL-58

(a) Four-parameter optical model

Potential	Strength of real part of nuclear optical potential, V, MeV	Strength of imaginary part of nuclear optical potential, W, MeV	Diffuseness parameter in Woods-Saxon potential, a, fm	Nuclear radius constant, r_o, fm	Total reaction cross section, σ_R, mb	Goodness of fit per data point, χ^2/N
A	75.41	19.50	0.615	1.48	1517	24.0
B	120.0	27.33	.635	1.39	1683	25.9
C	150.8	31.05	.624	1.36	1512	23.2

(b) Six-parameter optical model

Potential	Strength of real part of nuclear optical potential, V, MeV	Diffuseness of real part of nuclear optical potential, a_o, fm	Radius constant of real part of nuclear optical potential, r_o, fm	Strength of imaginary part of nuclear optical potential, W, MeV	Diffuseness of imaginary part of nuclear optical potential, a_i, fm	Radius constant of imaginary part of nuclear optical potential, r_i, fm	Total reaction cross section, σ_R, mb	Goodness of fit per data point, χ^2/N
D	41.45	0.684	1.52	10.07	0.559	1.71	1541	15.8
E	70.92	.582	1.50	26.21	.926	1.18	1594	14.9
F	139.3	.565	1.47	16.32	.275	1.71	1494	16.5
G	180.8	.548	1.45	18.63	.264	1.69	1496	17.2

angles less than 76°. For larger angles, either 10 percent or the statistical uncertainty, whichever was greater, was used.

A number of optical model search calculations were performed using four-parameter potentials whose initial values were chosen from the results of Broek et al. (ref. 17). They measured the elastic and inelastic cross sections for 43-MeV alpha particles scattered from ^{58}Ni and performed an extensive series of optical model calculations on the data. The results of the four parameter optical model search calculations performed on the 41-MeV scattering data presented here are listed in table III(a) and pictured in figures 7(a) to (c), where they are compared with the measured elastic angular distribution. Other equivalent optical potentials could no doubt be found. One notes that the quality of fit to the data is poor compared with fits obtained on nuclei in the tin region (refs. 1 and 2). Typically, at scattering angles greater than 90°, the calculated angular distributions are out of phase with the measured angular distribution.

Attempts were made to improve the fits to the elastic cross sections by performing calculations using the six-parameter optical potential of equation (4). A series of calculations was performed whereby the two potential strengths (V and W) and the two diffusenesses (a_o and a_i) were obtained by a four-parameter search. The two radii (r_o and r_i), although fixed during each calculation, were varied independently in successive calculations in steps of 0.04 femtometer within the limits.

$$1.31 \leq r_o \leq 1.75 \text{ fm}$$

and

$$1.43 \leq r_i \leq 1.79 \text{ fm}$$

Three such series of calculations were performed in which V and W were initially assumed to be 60 and 15 MeV, 150 and 35 MeV, and 200 and 15 MeV, respectively. For all calculations, the initial values of a_o and a_i were assumed to be 0.6 and 0.4, respectively. The parametric values that gave the best fits to the experimental data were then used as starting values for six-parameter search calculations. These potentials are listed in table III(b). The resultant calculated angular distributions are compared with the data in figures 7(d) to (g). They provide significantly better fits than calculations using four-parameter potentials. The overall goodness of fit, as measured by χ^2/N which is defined in equation (6), is similar for each of the several six-parameter potentials listed. However, the phases of the angular distributions calculated using these potentials with real well depths of 139.3 and 180.8 MeV are in better agreement with the data at angles greater than 110° than calculations using potentials with shallower real well depths.

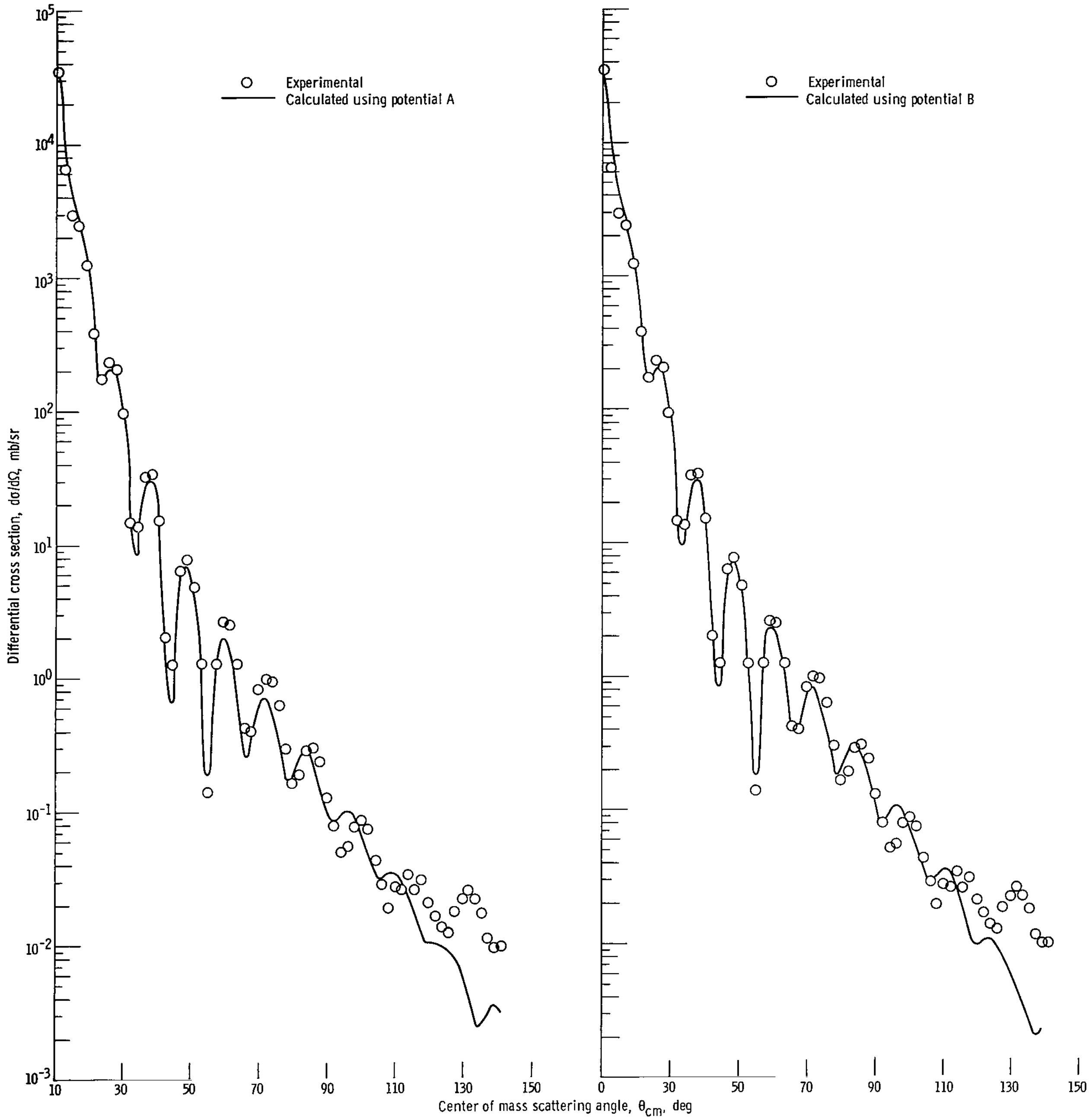

(a) Calculations using potential A.

(b) Calculations using potential B.

Figure 7. - Experimental and calculated elastic angular distributions of 41-MeV alpha particles scattered from nickel-58. (See table III for characteristics of potentials.)

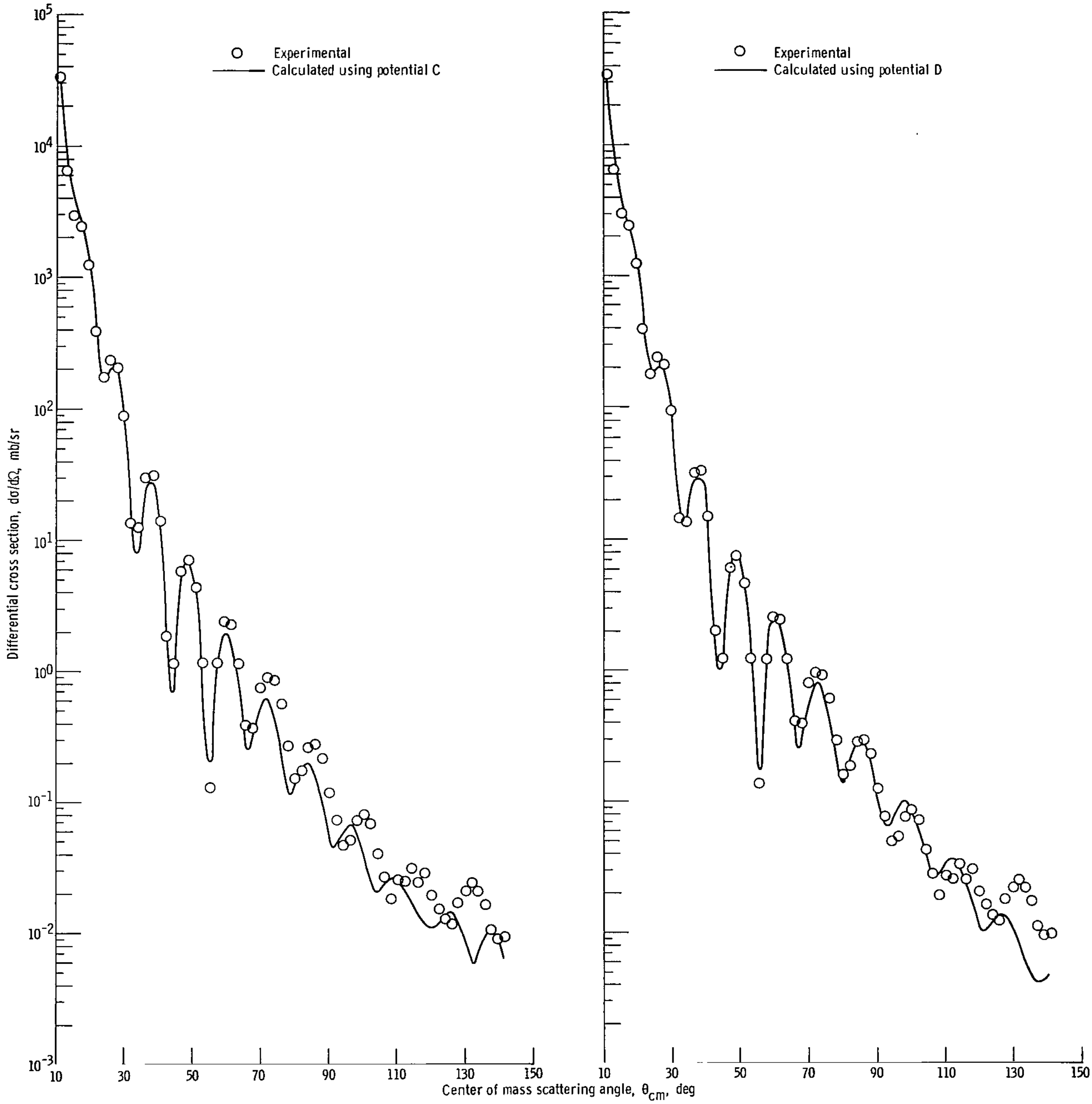

(c) Calculations using potential C.

(d) Calculations using potential D.

Figure 7. - Continued.

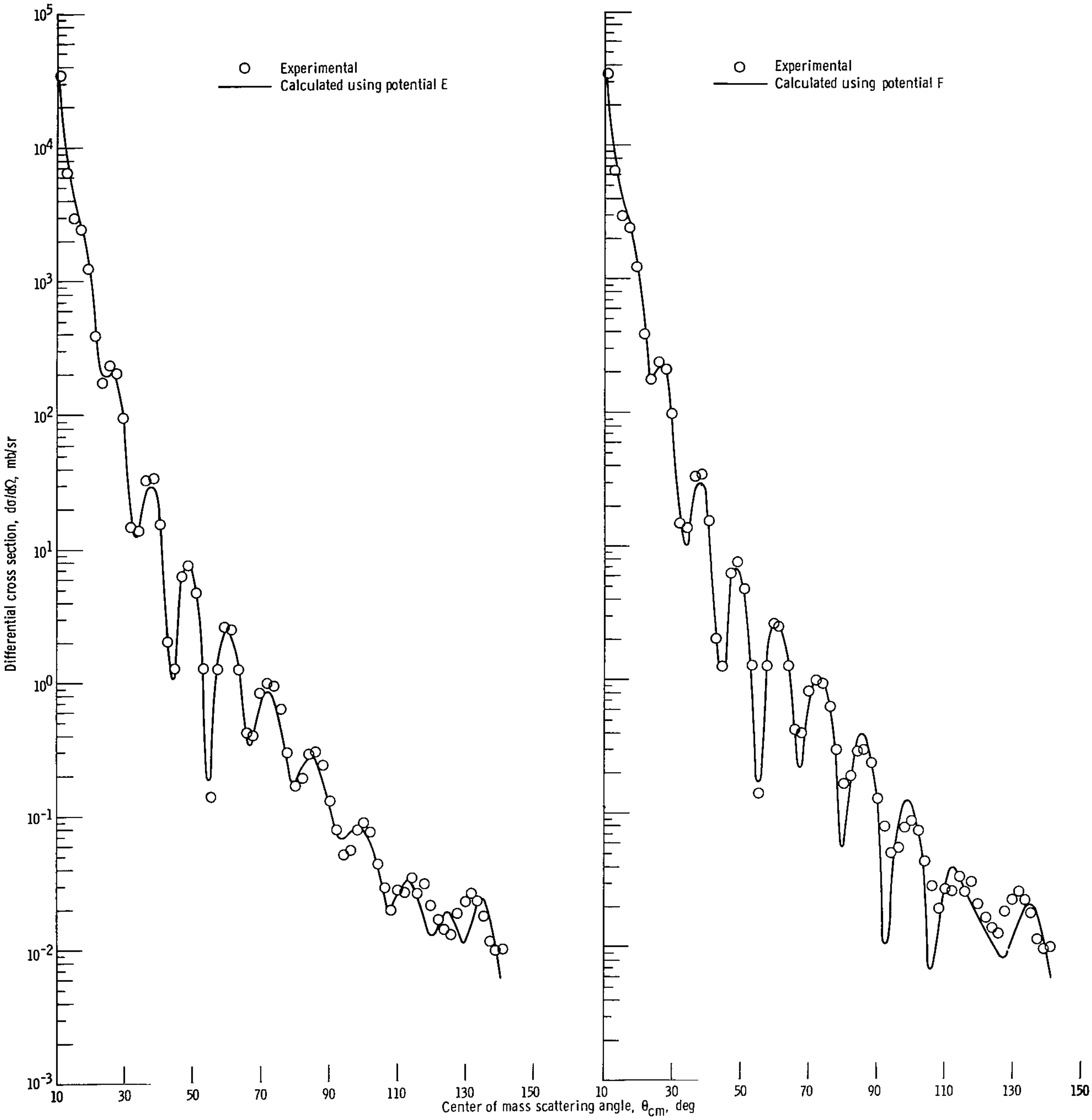

(e) Calculations using potential E.

(f) Calculations using potential F.

Figure 7. - Continued.

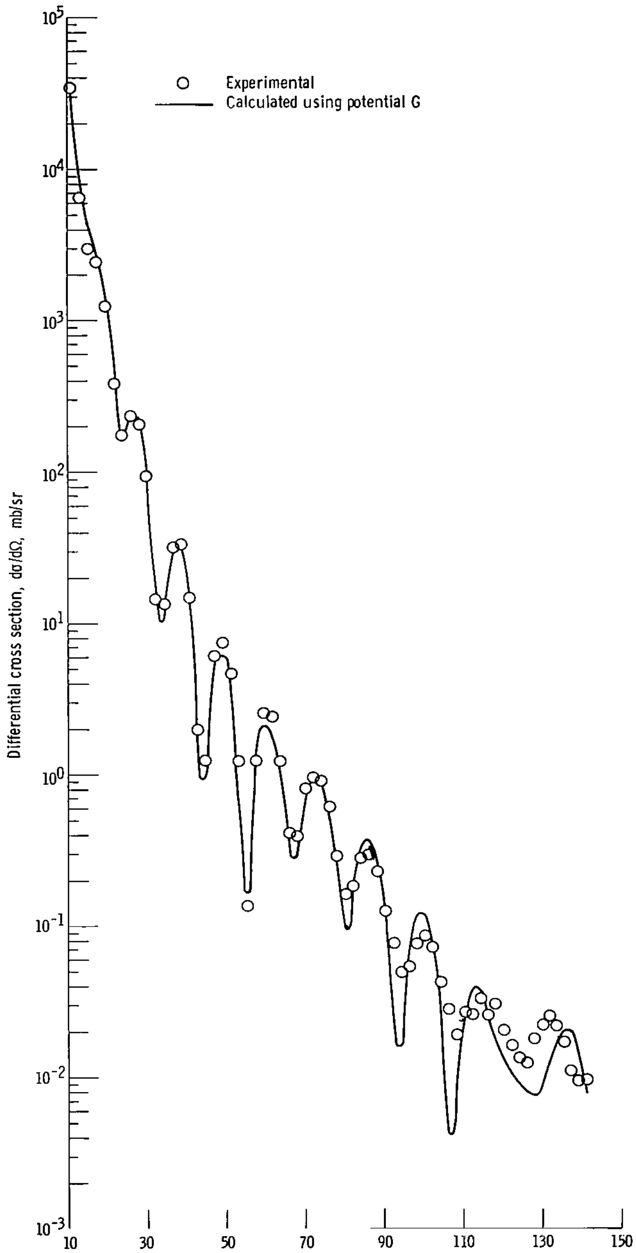

(g) Calculations using potential G.

Figure 7. - Concluded.

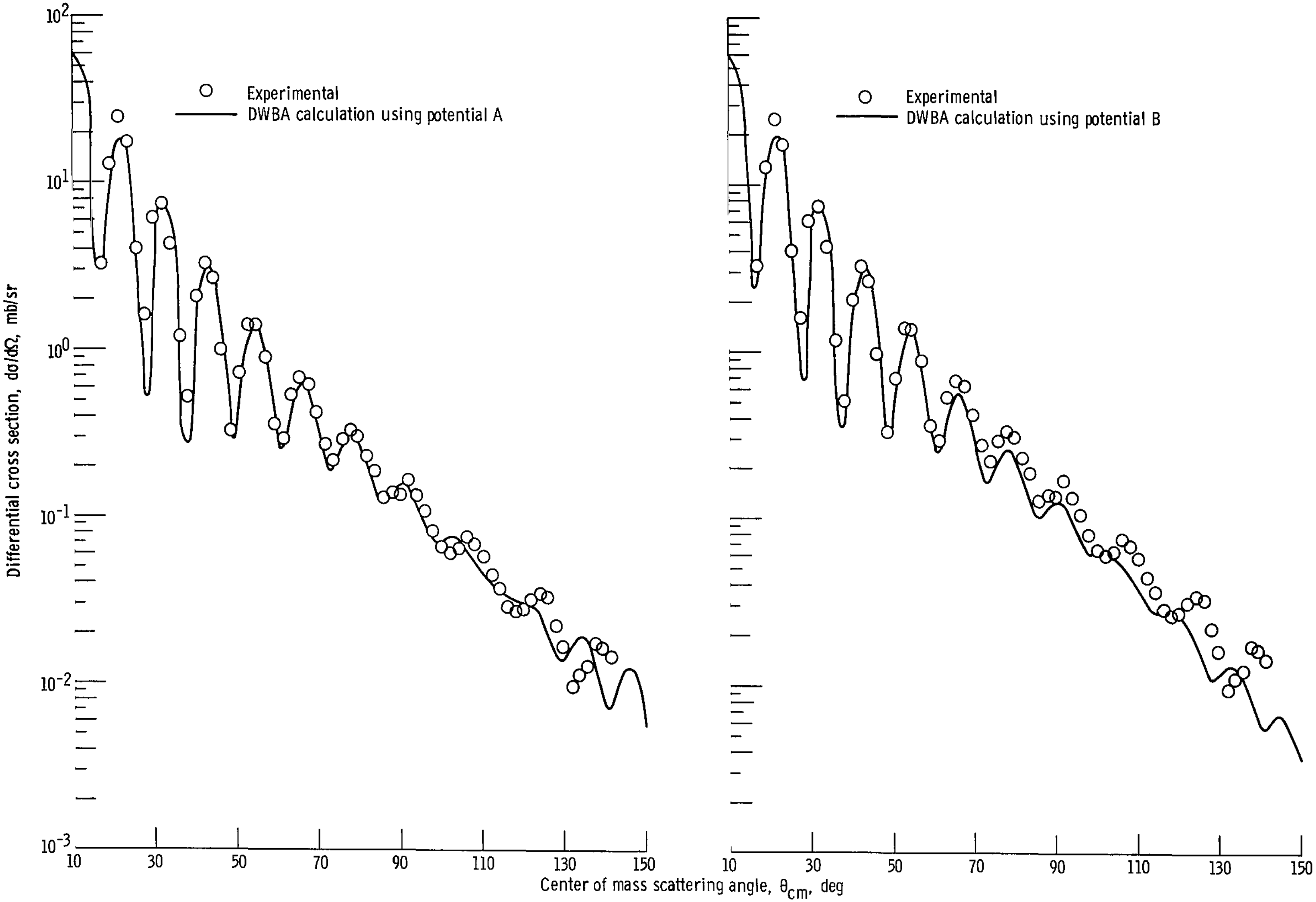

(a) Calculations using potential A; nuclear deformation parameter, 0.22.

(b) Calculations using potential B; nuclear deformation parameter, 0.24.

Figure 8. - Experimental and calculated inelastic angular distributions of 41-MeV alpha particles scattered from nickel-58. (See table III for characteristics of optical model potentials.

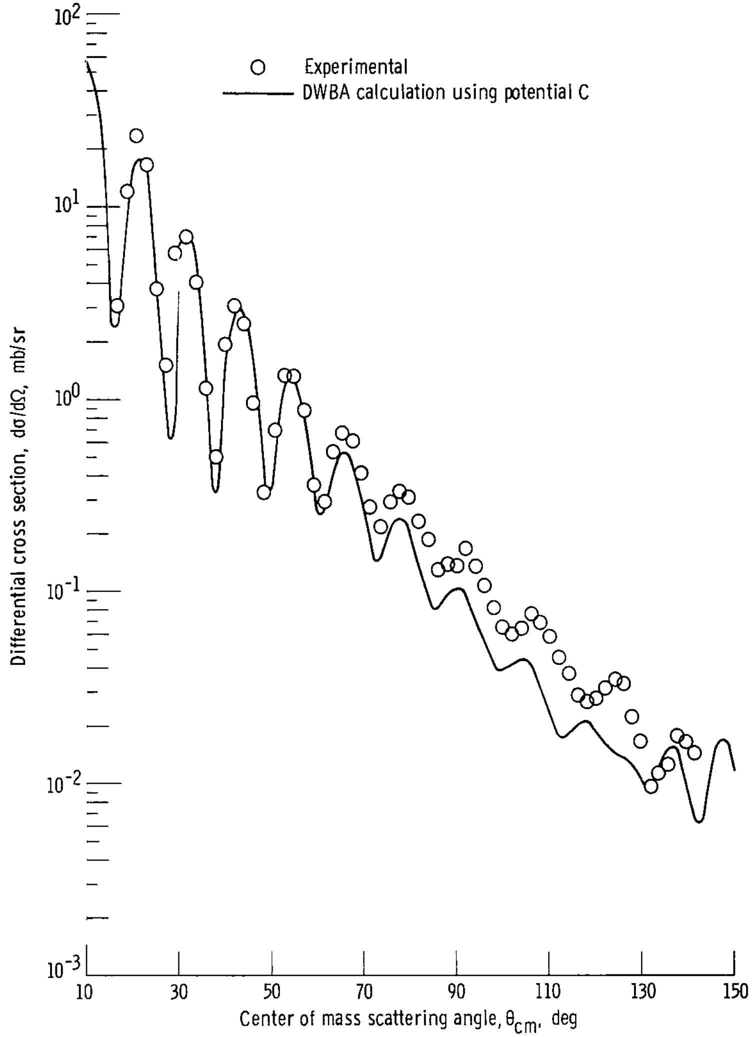

(c) Calculations using potential C; nuclear deformation parameter, 0.24.

Figure 8. - Continued.

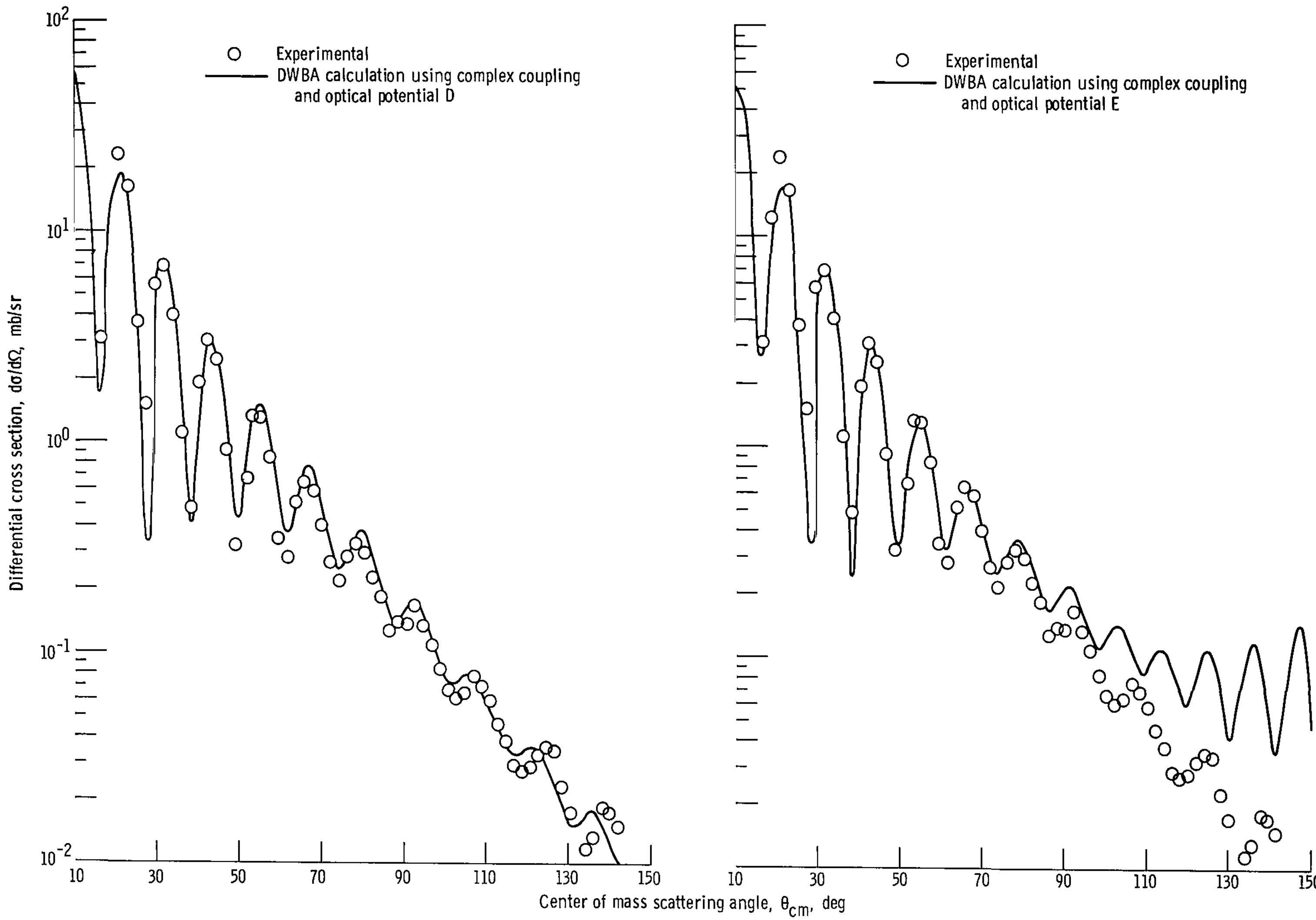

(d) Calculations using potential D; nuclear deformation parameter, 0.23.

(e) Calculations using potential E; nuclear deformation parameter, 0.22.

Figure 8. - Continued.

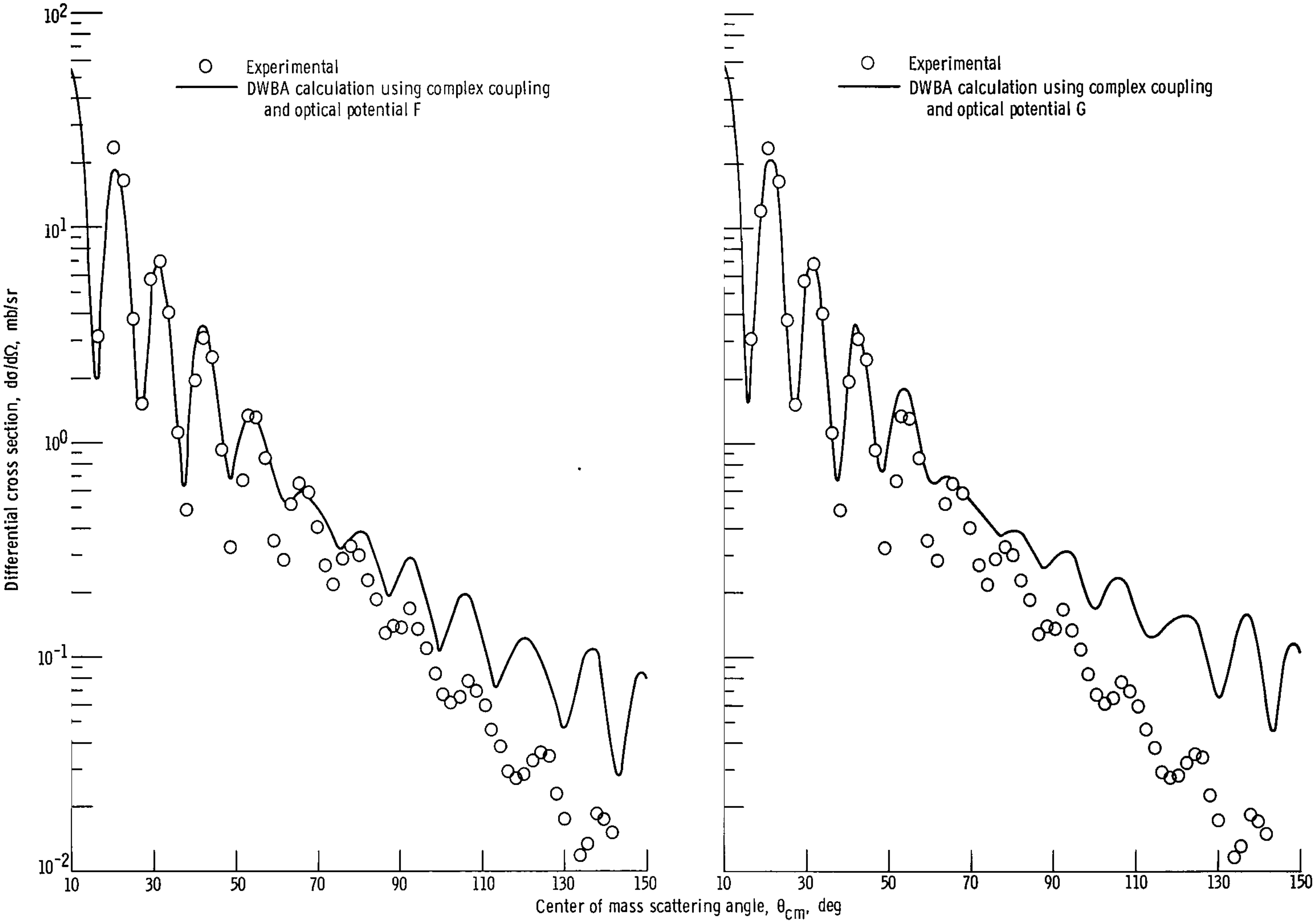

(f) Calculations using potential F; nuclear deformation parameter, 0.25.

(g) Calculations using potential G; nuclear deformation parameter, 0.25.

Figure 8. - Concluded.

Inelastic Cross-Section Analysis

Figures 8(a) to (c) show the measured 41-MeV alpha inelastic cross sections for excitation of the 1.452-MeV 2^+ level of ^{58}Ni compared with the results of DWBA calculations (ref. 18) using the four-parameter optical potentials of table III(a). Such a calculation assumes the optical model potential to be nonspherical, the elastic scattering determining the spherical part. The distorted waves method treats the nonspherical part to first order in the deformation or "deformability" β_l of the 2^l-pole mode. For all three potentials, the calculated 2^+ angular distributions are out of phase with the measured 2^+ angular distribution at angles greater than 90°. Deformation parameters β_2 were determined for each calculation by normalizing the calculated distribution to the measured cross section at 32° and are listed in table IV.

TABLE IV. - ANALYSIS OF 41-MeV ALPHA INELASTIC CROSS SECTIONS FOR EXCITATION TO THE 1.452-MeV LEVEL OF NICKEL-58

Potential	Nuclear deformation parameter,[a] β_2
A	0.22
B	.24
C	.24
D	.22
E	.23
F	.25
G	.25

[a]A value for β_2 of 0.214 ± 0.021 obtained from Coulomb excitation measurements has been reported (refs. 25 and 26).

In accordance with a suggestion by Broek et al. (ref. 17), DWBA calculations using complex coupling were performed using the six-parameter optical potentials listed in table III(b). With the exception of potential E, these potentials each have an imaginary radius greater than the real radius and an imaginary diffuseness smaller than the real diffuseness. This agrees with the findings of Broek et al. (ref. 17). Figures 8(d) to (g) show the results of these DWBA calculations compared with the measured 2^+ angular distribution. Deformation parameters β_2 were obtained as before by normalizing the calculated distribution to the measured cross section at 32° and are listed in table IV.

These values are similar to those obtained using four-parameter optical potentials.

The 2^+ angular distribution calculated using potential D is in excellent agreement with the measured cross sections out to 110° after which it gets slightly out of phase with the data. The 2^+ distribution calculated using potential E is seriously out of phase with the data at angles greater than 90°. The phases of the calculated angular distributions using potentials F and G are in reasonably good agreement with the data. However, with the exception of the calculation using potential D, the magnitudes of these calculated cross sections at back angles do not decrease as rapidly as the measured values. Furthermore, the peak to valley ratios of the diffraction patterns calculated using potentials F and G are not as large as the ratios obtained from the data in the angular region of 50° to 80°.

Analysis of Correlation Data

Figure 9 shows the experimentally measured values of the symmetry angles θ_0 compared with the symmetry angles calculated using the transition amplitudes obtained from DWBA calculations. The figure also shows the adiabatic prediction (refs. 19 and 20) where the symmetry angle θ_0 is the angle of adiabatic recoil of the target nucleus. The adiabatic approximation assumes that the energy of the scattered particle equals that of the incident particle. It is interesting to note that the measured values of θ_0 are close to the adiabatic predictions at $\theta_\alpha = 21^\circ$, 32°, 43°, and 54°, which are the regions of the diffraction maxima for the inelastic angular distributions. This is a phenomenon typical for all symmetry angle measurements made to date that include $^{12}C\ (\alpha, \alpha'\gamma_{4.433})$ (refs. 9 and 21), $^{24}Mg\ (\alpha, \alpha'\gamma_{1.37})$ (refs. 7 and 21), $^{120}Sn\ (\alpha, \alpha'\gamma_{1.176})$ (ref. 22), as well as $^{58}Ni\ (\alpha, \alpha'\gamma_{1.452})$ using 41- or 42-MeV incident alpha particles; and $^{12}C\ (\alpha, \alpha'\gamma_{4.433})$ (ref. 23), $^{24}Mg\ (\alpha, \alpha'\gamma_{1.37})$ (ref. 23), $^{28}Si\ (\alpha, \alpha'\gamma_{1.77})$ (ref. 24), and $^{56}Fe\ (\alpha, \alpha'\gamma_{0.84})$ (ref. 24) using 22.5-MeV incident alpha particles. Similarly, it has been observed that the existence of any symmetry angle structure (i.e, deviations from the adiabatic prediction due to rapid reverse or forward rotations) occurs at alpha scattering angles where the 2^+ cross sections are a minimum. The small cross sections make it difficult to measure the alpha-gamma correlation pattern with good statistical accuracy. This results in large experimental uncertainties at just those alpha scattering angles where the best experimental accuracy is desired. However, particularly long bombardments were made in the angular region of θ_α between 25° and 30° to reduce the statistical uncertainty of θ_0 in this region. All the calculated symmetry angles shown in these figures display a very rapid reverse rotation in the region of alpha scattering angles of 17° and 27.5° in agreement with the data. At these alpha scattering angles, the calculated reverse rotations of the

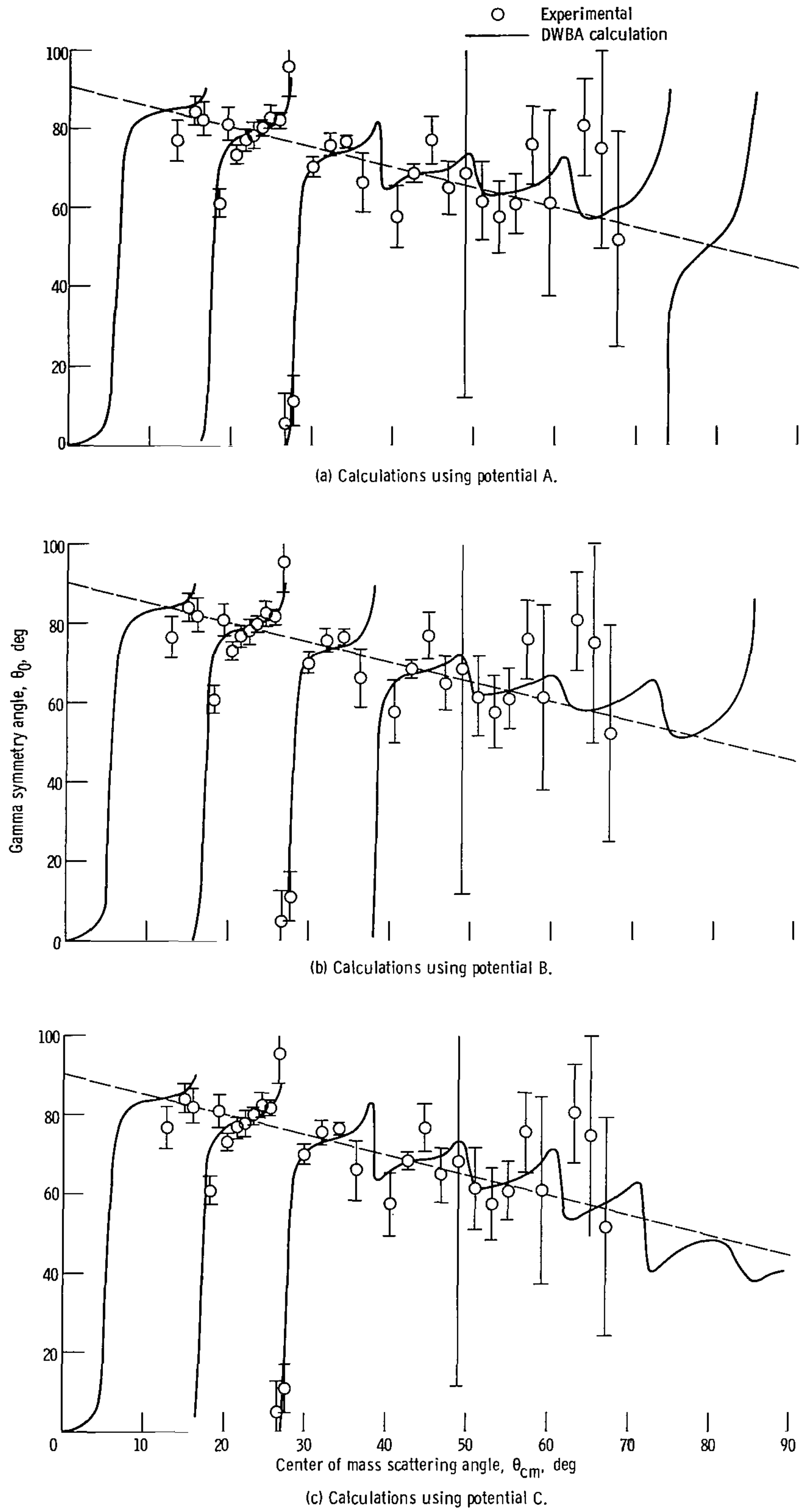

Figure 9. - Experimental and calculated gamma symmetry angles for reaction $^{58}Ni(\alpha,\alpha'\gamma_{1.452})^{58}Ni$. (See table III for characteristics of optical model potentials.)

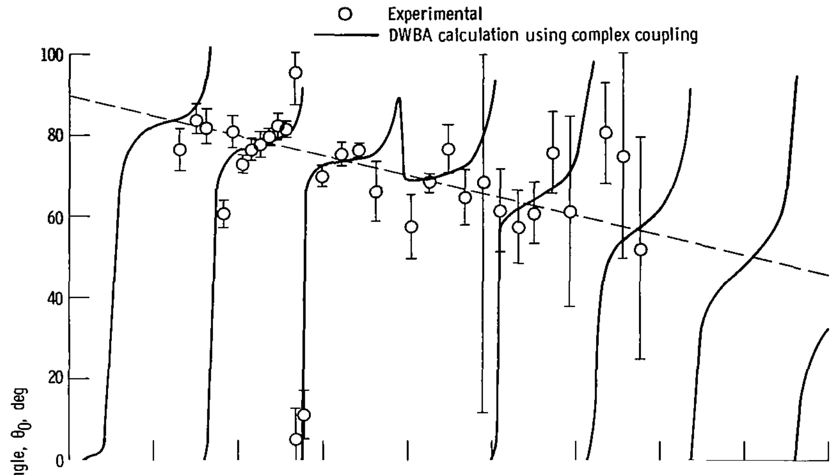

(d) Calculations using potential D.

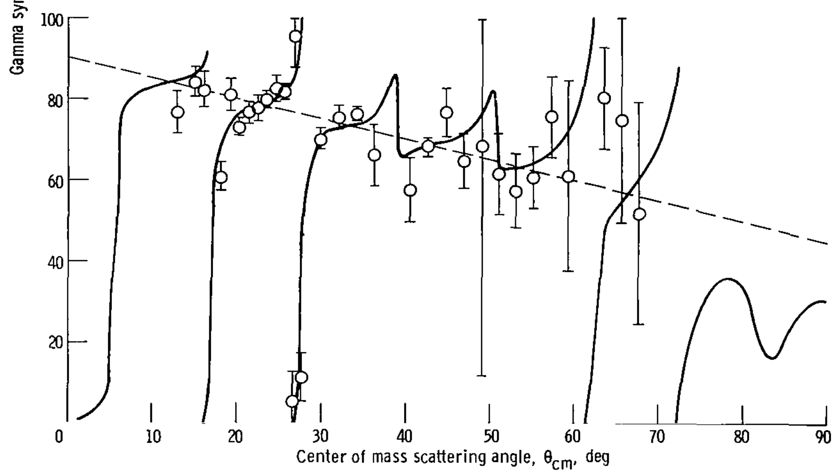

(e) Calculations using potential E.

Figure 9. - Continued.

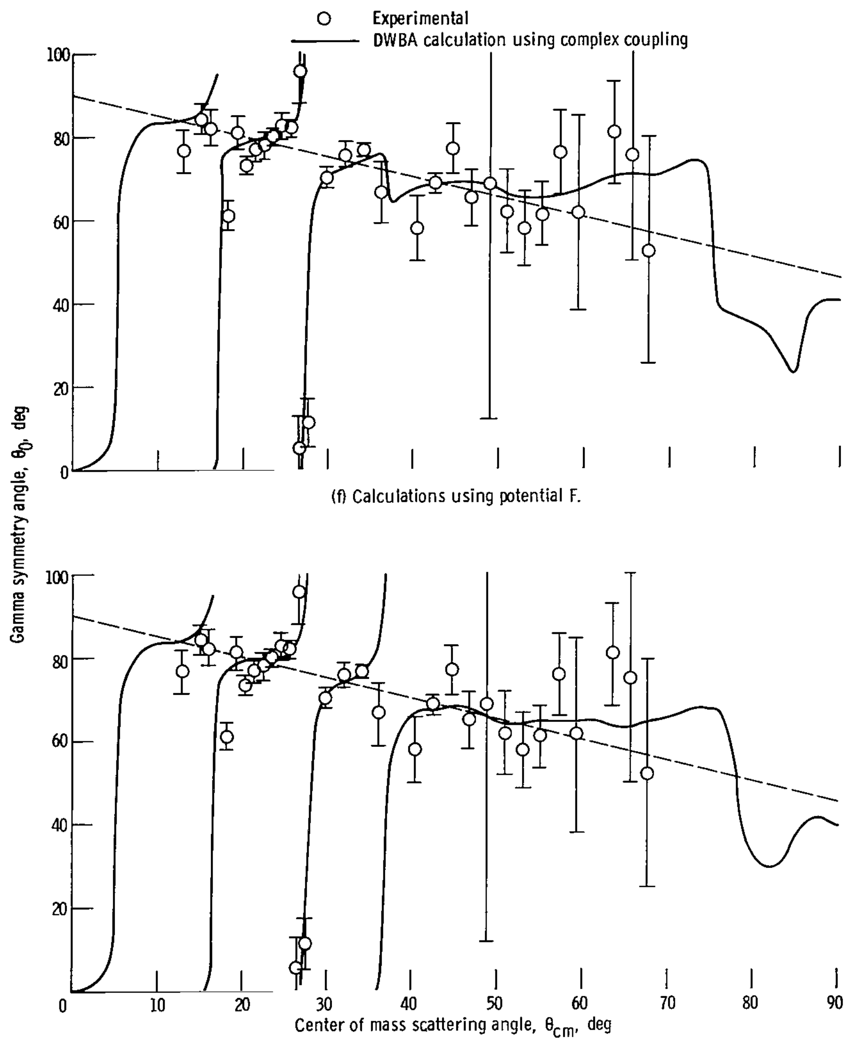

(f) Calculations using potential F.

(g) Calculations using potential G.

Figure 9. - Concluded.

symmetry angles are as rapid as 70^{o} over only 0.5^{o} variation of the alpha scattering angle. Consequently, an angular resolution for the alpha detectors of 0.25^{o} was used at these angles in order to observe such rapid rotations.

DISCUSSION

The four-parameter optical potentials (table III(a)) predict similar elastic cross sections. In general, the phases and magnitudes are in poor agreement with the data at angles greater than 90^{o}. Similarly, DWBA calculations of the 2^{+} cross sections agreed poorly with the data at angles larger than 90^{o}. However, those cross sections calculated using potential A were in better agreement than calculations using potentials B and C. The deformation parameters β_2 listed in table IV and predicted by all three calculations agree very well with the quoted experimental value of 0.214±0.021 obtained from Coulomb excitation measurements (refs. 25 and 26). In addition, potentials A to C resulted in calculated symmetry angles that agree with the experimental values in regions where very rapid reverse rotations are observed, that is, at alpha scattering angles of about 17^{o} and 27.5^{o}.

The elastic cross sections calculated using the six-parameter optical potentials (table III(b)) result in significantly better fits to the elastic data than were obtained using the four-parameter potentials. In particular, calculations using potentials F and G, which have real well depths of 139 and 181 MeV, respectively, result in reasonably good phase agreement with the data as far back as 140^{o}. However, the phases of the angular distributions and the magnitudes of the 2^{+} cross sections calculated using complex coupling agree best with the data using potential D, which has a real well depth of 41.5 MeV. The deformation parameters β_2 predicted by these calculations agree reasonably well with the measured value. Also, using the six-parameter potentials, calculations predict the measured rapid reverse rotations of θ_0 at alpha scattering angles of about 17^{o} and 27.5^{o}. These are similar to the results of the four-parameter potential calculations.

Beyond 27.5^{o}, the different potentials show different characteristic symmetry angle rotations at the alpha scattering angles where the 2^{+} cross sections are at a minimum. Among the four-parameter potentials, use of potential C predicts no rapid reverse rotations beyond 27.5^{o}. However, use of potential B shows other rapid reverse rotations at 38^{o} and 86^{o}, whereas use of potential A predicts other rapid reverse rotations at 74^{o} and 86^{o}. Among the six-parameter potentials, use of potential F predicts beyond 27.5^{o} no other rapid reverse rotations, but use of potential G predicts another rotation at 38^{o}. Use of potentials D and E each result in several additional rapid rotations from 49^{o} on back.

In Blair's generalized "Fraunhofer" treatment of the inelastic diffraction model (ref. 19) the expression

$$2\,kR \sin \frac{\theta}{2}$$

locates the peaks and valleys of the angular distribution. It is interesting to note that this expression has a value at the alpha scattering angle of 27.5° equal to that calculated at those alpha scattering angles where the last rapid reverse symmetry angle rotation occurs for similar measurements on ^{12}C (ref. 9) and ^{120}Sn (ref. 22). At larger alpha scattering angles and where the 2^{+} cross sections are a minimum, the measured values of the ^{12}C and ^{120}Sn symmetry angles indicate that the rotations are small and in the forward direction, similar to the results of symmetry angle calculations shown in figures 9(c) and (f) using potentials C and F, respectively. However, no definite conclusions can be drawn from the ^{58}Ni data because symmetry angle measurements at the significant alpha scattering angles do not exist beyond 27.5°.

The reaction, or absorption, cross sections σ_R predicted by the optical model fits discussed here are listed in table III. The measured cross section at 40 MeV is 1354±57 millibarns (ref. 27). Potentials A and C, among the four-parameter potentials, have values that are included by 1514±3 millibarns, and potentials F and G, among the six-parameter potentials, have values that are included by 1495±1 millibarns. Considering the upper limit of the measured value, these calculated cross sections are approximately 7 percent too large. The reason for this discrepancy is unclear.

On the basis of the data presented here, one cannot choose from the several optical potentials used in this analysis any particular one as being superior to the others for describing the cross section and symmetry angle data using a macroscopic collective model. Giving consideration to the phases of the elastic angular distributions at large angles, the best description of the elastic cross sections is obtained using the six-parameter potential F, which has a real well depth of 139 MeV. The best agreement with the measured 2^{+} cross sections is obtained using the six-parameter potential D, which has a real well depth of 41.5 MeV. All the potentials used in the analysis predict similar symmetry angles for alpha scattering angles as large as 30°.

Lewis Research Center,
National Aeronautics and Space Administration,
Cleveland, Ohio, September 17, 1969,
129-02.

REFERENCES

1. Baron, Norton; Leonard, Regis F.; Need, John L.; and Stewart, William M.: Elastic and Inelastic Scattering of 40-MeV Alpha Particles From Even Tin Isotopes. NASA TN D-3067, 1965.

   Baron, N.; Leonard, R. F.; Need, J. L.; Stewart, W. M.; and Madsen, V. A.: Inelastic Alpha Particle Excitation in the Even Tin Isotopes. Phys. Rev., Vol. **146**, No. 3, June 17, 1966, pp. 861-8.

2. Leonard, Regis F.; Stewart, William M.; and Baron, Norton: Elastic and Inelastic Scattering of 42-MeV Alpha Particles From Even Tellurium Isotopes. NASA TN D-3991, 1967.

   Leonard, R. F.; Stewart, W. M.; and Baron, N.: Alpha-Particle Scattering From Even Tellurium Isotopes. Phys. Rev., Vol. 162, No. 4, October 20, 1967, pp. 1125-9.

3. Austern, N.: Optical Model Wave Functions for Strongly Absorbing Nuclei. Annals Phys., Vol. 15, No. 3, Sept. 1961, pp. 299-313.

4. Drisko, R. M.; Satchler, G. R.; and Bassel, R. H.: Ambiguities in the Optical Potential for Strongly Absorbed Projectiles. Phys. Letters, Vol. 5, No. 5, Aug. 1, 1963, pp. 347-50.

5. Bassel, R. H.; Satchler, G. R.; Drisko, R. M.; and Rost, E.: Analysis of the Inelastic Scattering of Alpha Particles. I. Phys. Rev., Vol. 128, No. 6, Dec. 15, 1962, pp. 2693-2707.

6. Rost, E.: Analysis of the Inelastic Scattering of Alpha Particles. II. Phys. Rev. Vol. 128, No. 6, Dec. 15, 1962, pp. 2708-16.

7. Leonard, Regis F.; Stewart, William M.; Baron, Norton N.; and Braley, Richard C.: Gamma Ray Angular Correlations Following Inelastic Scattering of 42-MeV Alpha Particles from Magnesium 24. NASA TN D-4683, 1968.

8. Baron, Norton; and Kaminski, Gerald A.: Manufacture of Lithium-Drifted Silicon Surface-Barrier Semiconductor Counters. NASA TN D-3554, 1966.

9. Stewart, W. M.; Baron, N.; Braley, R. C.; and Leonard, R. F.: Alpha-Gamma Angular Correlations in the Reaction Carbon-12 $(\alpha, \alpha' \gamma_{4.433\mathrm{MeV}})$. NASA TN D-5568.

10. Williamson, C.; and Boojot, J. P.: Tables of Range and Rate of Energy Loss of Charged Particles of Energy 0.5 to 150 MeV. Rept. No. CEA-2189, Centre d-Etudes Nucleaires, Saclay, 1963.

11. Tobocman, William: Theory of Direct Nuclear Reactions. Oxford Univ. Press, 1961.

12. Banerjee, Manoj K.; and Levinson, Carl A.: Direct Interaction Theory of Inelastic Scattering. Part II. Angular Correlation of Gamma Rays Following Inelastic Scattering. Annals. Phys., Vol. 2, No. 5, Nov. 1957, pp. 499-524.

13. Rose, M. E.: The Analysis of Angular Correlation and Angular Distribution Data. Phys. Rev., Vol. 91, No. 3, Aug. 1, 1953, pp. 610-15.

14. Hodgson, Peter E.: The Optical Model of Elastic Scattering. Oxford Univ. Press, 1963.

15. Melkanoff, Michael A.; Nodvik, John S.; Saxon, D. S.; and Cantor, D. G.: A FORTRON Program for Elastic Scattering Analyses with the Nuclear Optical Model. Univ. Calif. Press, 1961.

16. Davidon, William C.: Variable Metric Method for Minimization. Rept. ANL-5990, (Ref.) Argonne National Lab., Nov. 1959.

17. Broek, H. W.; Yntema, J. L.; Buck, B.; and Satchler, G. R.: Wide-Angle Scattering of 43-MeV Alpha Particles by ^{58}Ni. Nucl. Phys., Vol. 64, 1965, pp. 259-72.

18. Gibbs, W. R.; Madsen, V. A.; Miller, J. A.; Tobacman, W.; Cox, E. C.; and Mowry, L.: Direct Reaction Calculation. NASA TN D-2170, 1964.

19. Blair, John S.: Inelastic Diffraction Scattering. Phys. Rev., Vol. 115, No. 4, Aug. 15, 1959, pp. 928-38.

20. Blair, J. S.; and Wilets, L.: Gamma Ray Correlation Function in the Adiabatic Approximation. Phys. Rev., Vol. 121, No. 4, Mar. 1, 1961, pp. 1493-9.

21. Hendrie, David L.: A Study of Coincidences Between Inelastically Scattered 42-MeV Alpha Particles and De-Excitation Gamma Rays. Ph.D. Thesis, Univ. Washington, 1964.

22. Leonard, R. F.; Stewart, W. M.; and Baron, N.: Gamma Ray Angular Correlations Following Inelastic Scattering of 42-MeV Alpha Particles From Tin-120. NASA TN D-5569.

23. Eidson, W. W.; Cramer, J. G., Jr.; Blatchley, D. E.; and Bent, R. D.: Angular Correlation Studies of Nuclear Polarization Following Inelastic Scattering of Alpha Particles from C^{12} and Mg^{24}, Nucl. Phys., Vol. 55, No. 4, 1964, pp. 613-42.

24. Cramer, J. G., Jr.; Eidson, W. W.; and Blatchley, D. E.: Angular-Correlation Studies of the Inelastic Scattering of Alpha Particles From C^{12}, Mg^{24}, Si^{28}, and Fe^{56}. Nuclear Spectroscopy with Direct Reactions. I. Contributed papers, F. E. Throw, Ed. Rept. No. ANL-6848, Argonne National Lab., Mar. 1964, pp. 153-8.

25. Stelson, P. H.; and McGowan, F. K.: Coulomb Excitation of the First 2^+ State of Even Nuclei with $58 \leq A \leq 82$. Nucl. Phys., Vol. 32, No. 4, May 1962, pp. 652-68.

26. Owen, L. W.; and Satchler, G. R.: Multipole Moments of a Rounded Charge-Distribution. Nucl. Phys., Vol. 51, No. 1, Feb. 1964, pp. 155-60.

27. Igo, G.; and Wilkins, B. D.: Alpha-Particle Reaction Cross Sections at 40 MeV. Phys. Rev., Vol. 131, No. 3, Aug. 1, 1963, pp. 1251-3.